

Astroparticle Physics

2022/23

1. **Historical introduction - basic properties of cosmic rays**
2. **Hadronic interactions and accelerator data**
3. **Cascade equations**
4. **Electromagnetic cascades**
5. **Extensive air showers**
6. **Detectors for extensive air showers**
7. **High-energy cosmic rays and the knee in the energy spectrum of cosmic rays**
8. **Radio detection of extensive air showers**
9. **Acceleration, Astrophysical accelerators and beam dumps**
10. **Extragalactic propagation of cosmic rays**
11. **Ultra-high-energy energy cosmic rays**
12. **Astrophysical gamma rays and neutrinos**
13. **Neutrino astronomy**
14. **Gamma-ray astronomy**

lecture 5

Extensive air showers

Gaisser chapter 16

16 Extensive air showers

- 16.1 Basic features of air showers
- 16.2 The Heitler–Matthews splitting model
- 16.3 Muons in air showers
- 16.4 Nuclei and the superposition model
- 16.5 Elongation rate theorem
- 16.6 Shower universality and cross section measurement
- 16.7 Particle detector arrays
- 16.8 Atmospheric Cherenkov light detectors
- 16.9 Fluorescence telescopes
- 16.10 Radio signal detection

Extensive Air Shower

Proton 10^{15} eV:
on ground

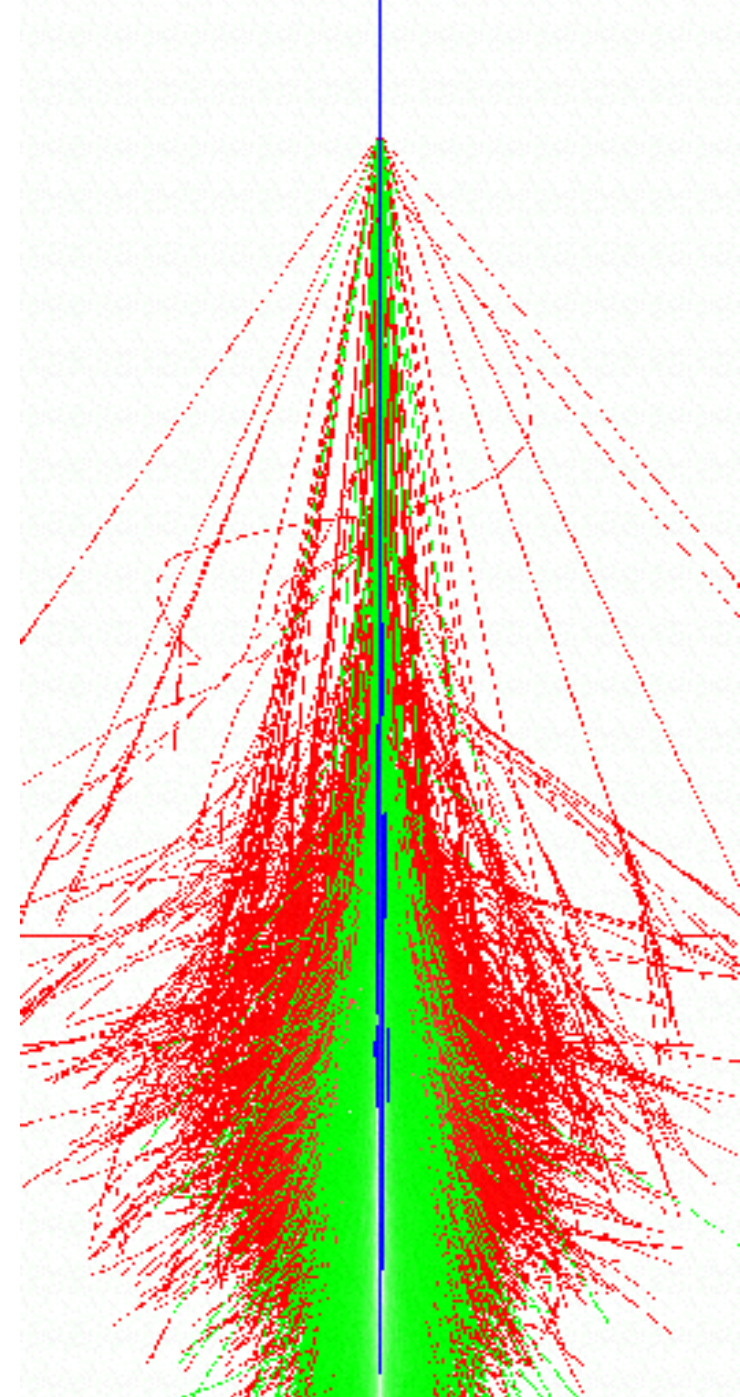
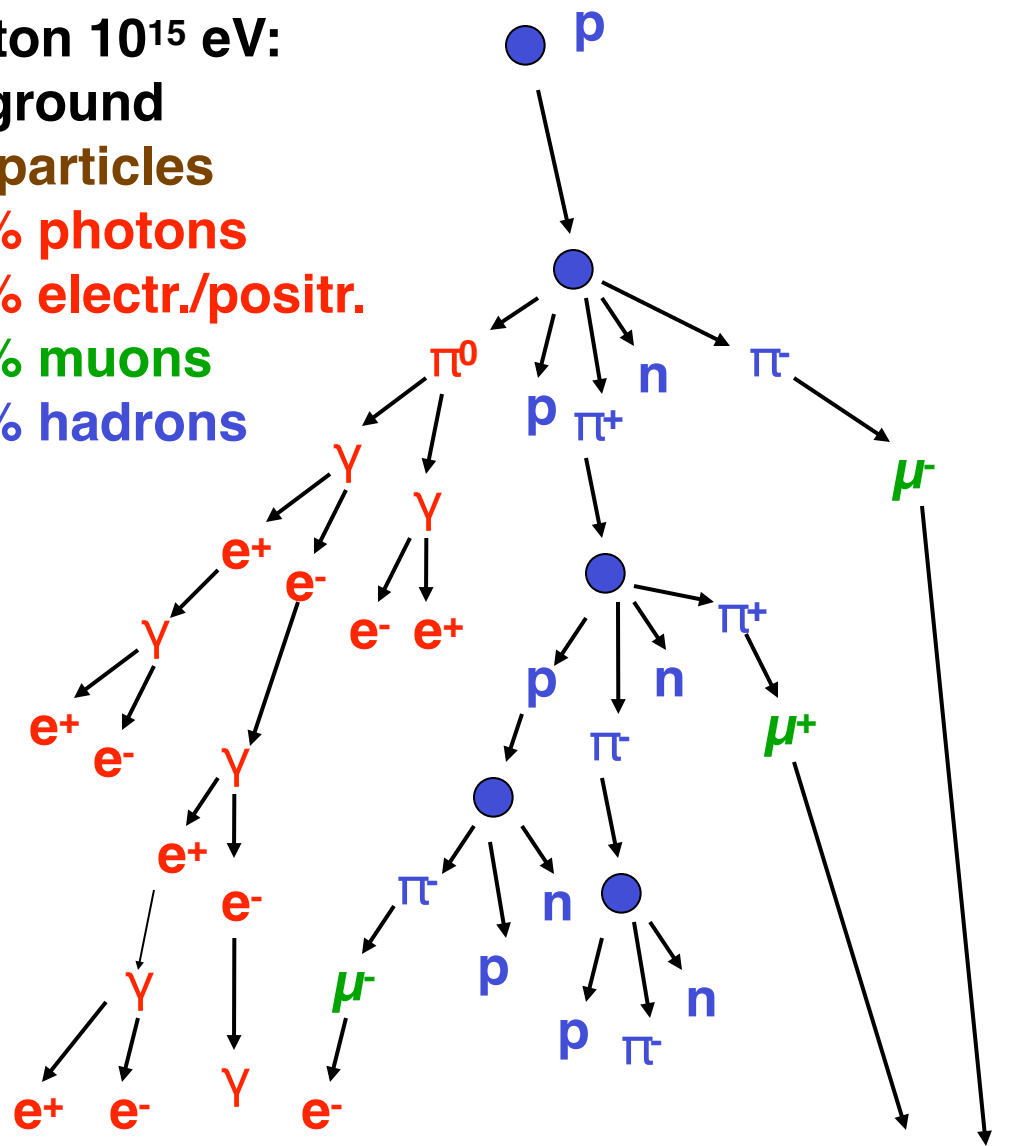
10^6 particles

80% photons

18% electr./positr.

1.7% muons

0.3% hadrons



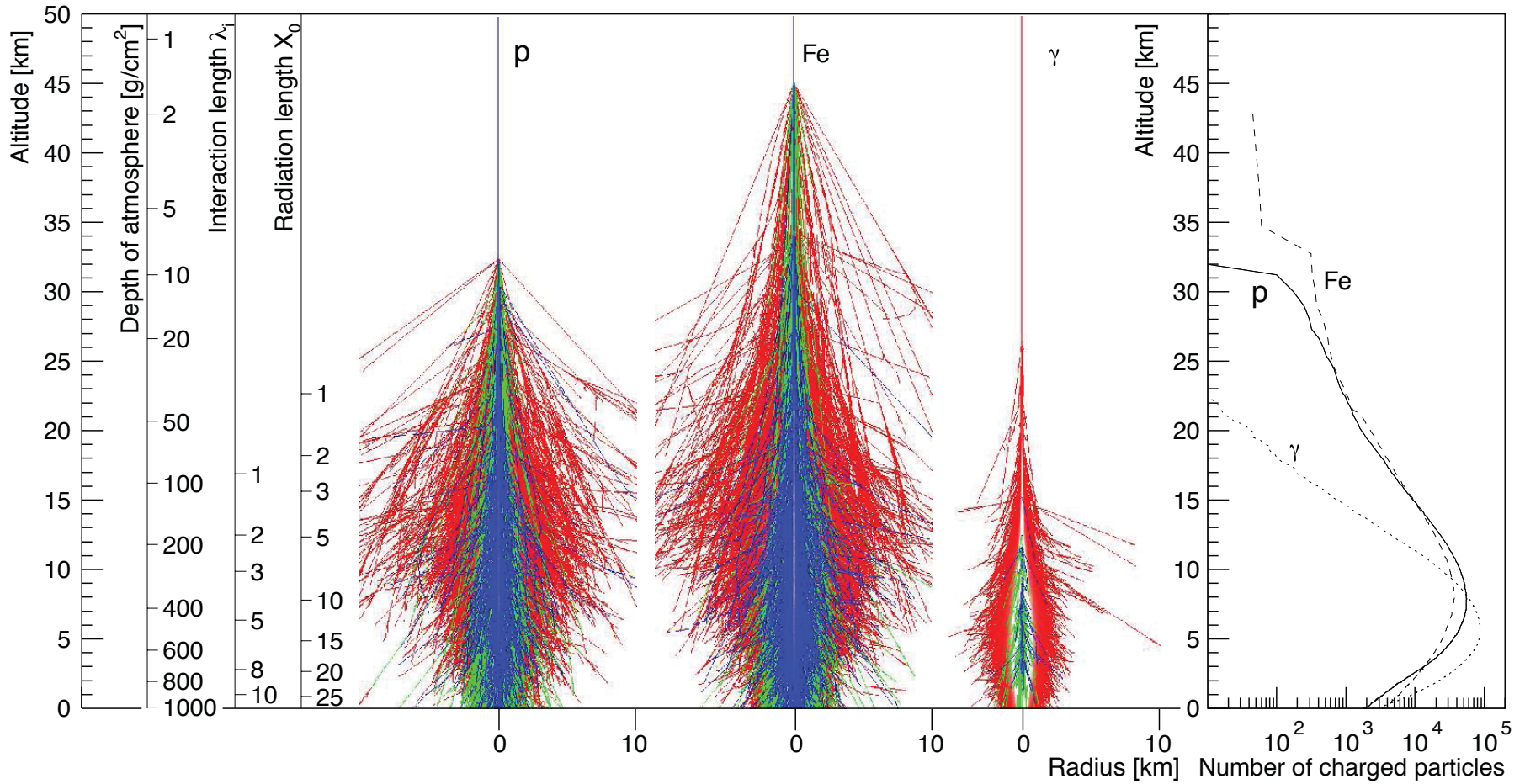
electromagnetic

hadronic

muonic

shower component

examples of showers with same (total) energy



16.1 Basic features of air showers

At each hadronic interaction, slightly more than a third of the energy goes into the electromagnetic component. Since most hadrons re-interact, most of the primary energy eventually finds its way into the electromagnetic component. In addition, because of the rapid multiplication of electromagnetic cascades, electrons and positrons are the most numerous charged particles in cosmic ray air showers. Thus, most of the shower energy is eventually dissipated by ionization losses of the electrons and positrons. It is correct to think of the atmosphere as a calorimeter to be sampled by the air shower detector. Apart from the small fraction, $F(E_0)$, of energy lost to neutrinos, the primary energy, E_0 is given by the *track length integral*,

$$(1 - F) \times E_0 \sim \alpha \times \int_0^{\infty} dX N(X), \quad (16.1)$$

where $N(X)$ is the number of charged particles in the shower at depth X (measured along the shower axis) and α is the energy loss per unit path length in the atmosphere averaged over all electron energies ($\alpha \approx 2.5 \text{ MeV}/(\text{g}/\text{cm}^2)$). In practice the track length integral must be extrapolated beyond the slant depth at the ground to account for energy remaining in the shower when it reaches the surface.

Energy measurement - calorimeter

hadron calorimeter

longitudinal shower development

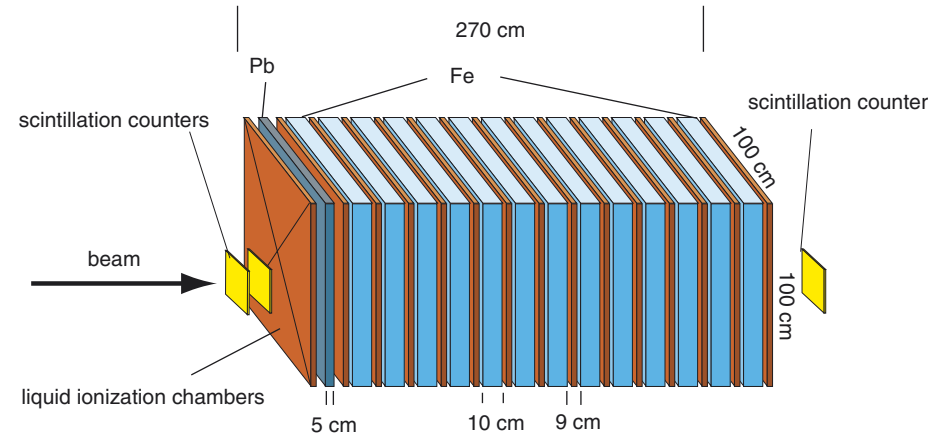


Fig. 2. Schematic view of the sampling calorimeter.

S. Plewnia et al. / Nuclear Instruments and Methods in Physics Research A 566 (2006) 422–432

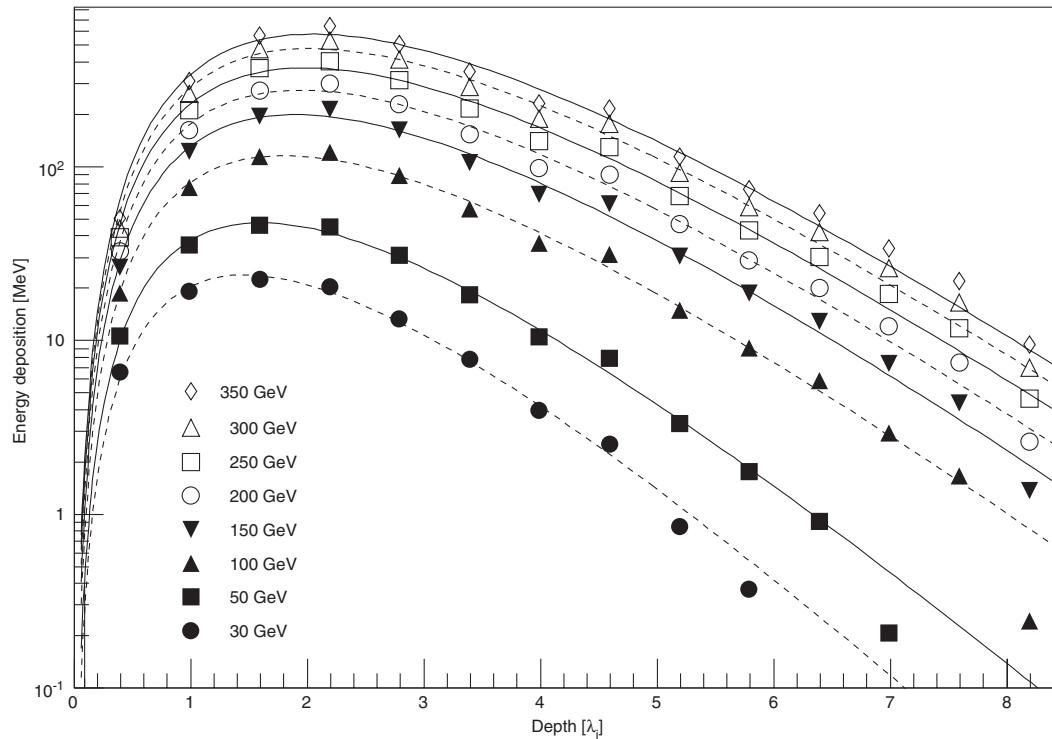


Fig. 13. Measured energy deposition as function of depth in the calorimeter for hadrons with energies from 30 to 350 GeV. The lines represent fits according to Eq. (7).

sampling calorimeter
alternating layers of absorber
material and detectors

energy resolution

$$\frac{\sigma(e)}{E} = A + B \frac{1}{\sqrt{E}}$$

$$E_{\text{dep}}(t) = A \cdot t^B \cdot \exp(-t/C)$$

Energy measurement - calorimeter

hadron calorimeter

lateral shower development

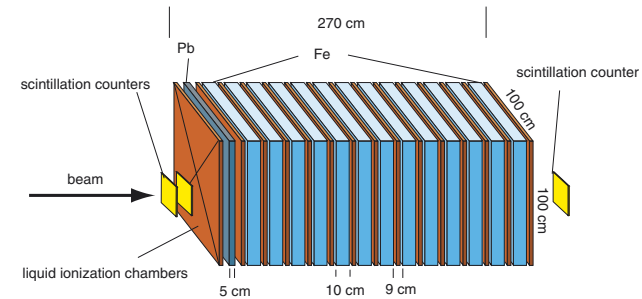
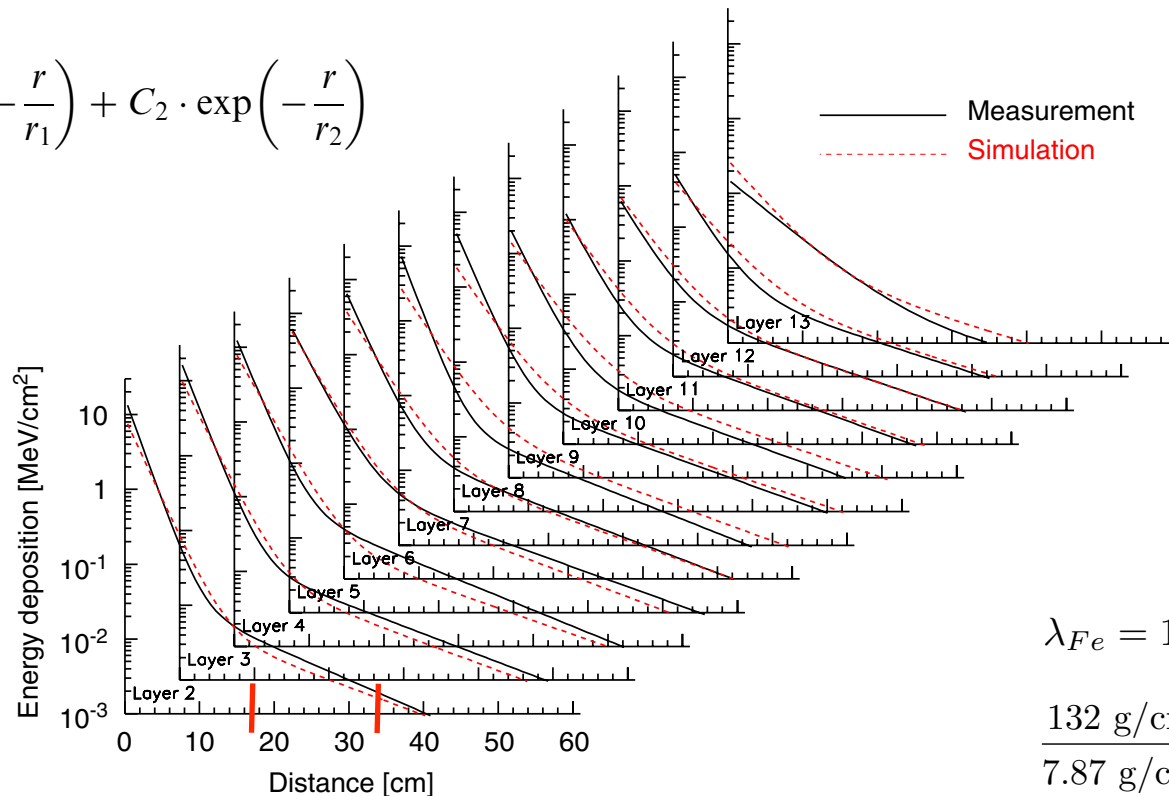


Fig. 2. Schematic view of the sampling calorimeter.

S. Plewnia et al. / Nuclear Instruments and Methods in Physics Research A 566 (2006) 422–432

427

$$\delta E(r) = C_1 \cdot \exp\left(-\frac{r}{r_1}\right) + C_2 \cdot \exp\left(-\frac{r}{r_2}\right)$$



$$\lambda_{Fe} = 132 \text{ g/cm}^2$$

$$\frac{132 \text{ g/cm}^2}{7.87 \text{ g/cm}^3} \approx 16.8 \text{ cm}$$

Fig. 9. Lateral distribution of the energy deposition in different layers of the calorimeter for 300 GeV hadrons. Measurements (solid lines) and simulations (dashed lines) are represented by parameterizations according to Eq. (5).

Energy measurement - calorimeter

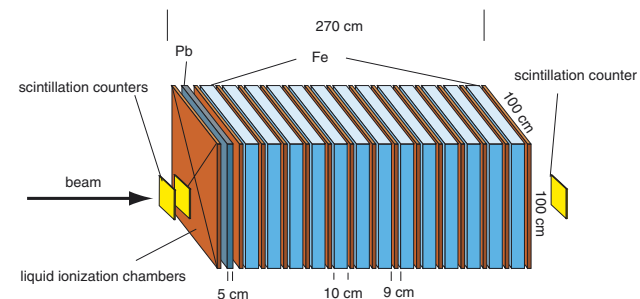


Fig. 2. Schematic view of the sampling calorimeter.

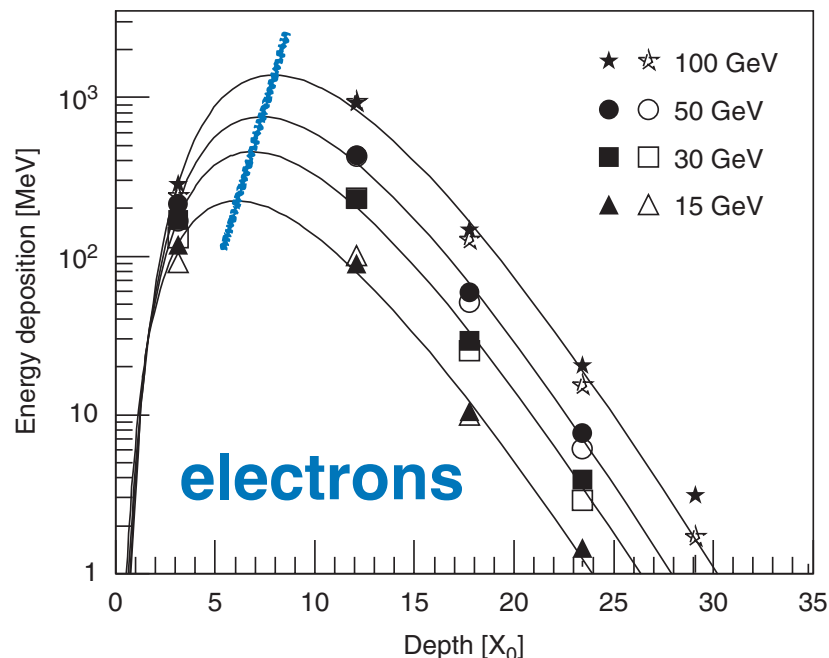


Fig. 16. Energy deposition as function of depth in the calorimeter for electrons. Shown are measurements (filled symbols) and results of simulations (open symbols). The lines represent fits to the measurements according to Eq. (7).

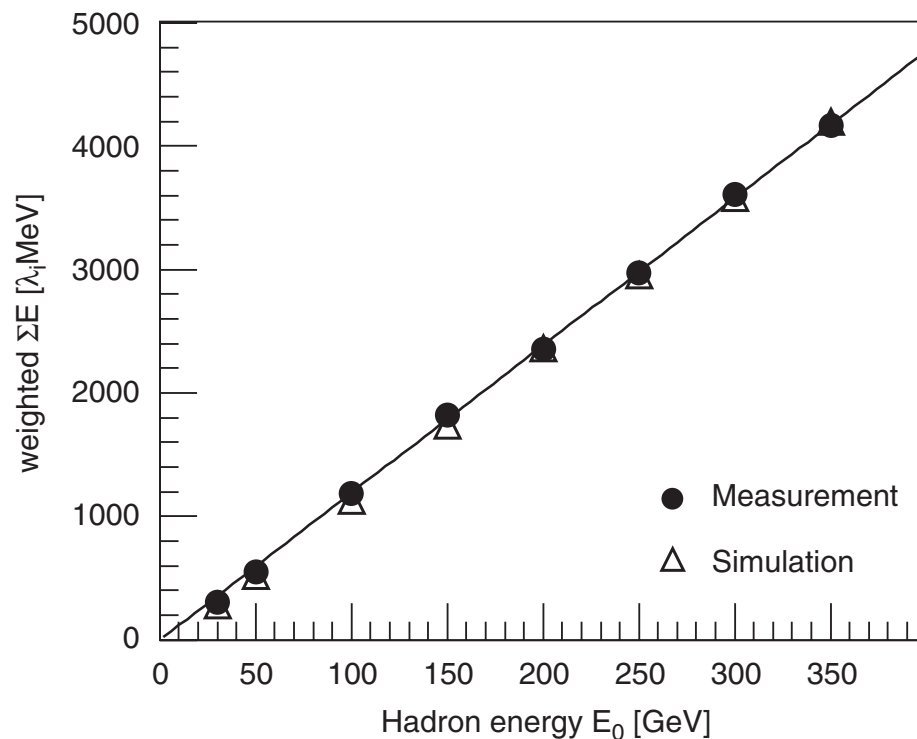


Fig. 17. Energy sum in the calorimeter as function of the incident hadron energy. The energy in each layer is weighted with the amount of absorber in front of the layer.

The data points have been fitted using the approach

$$E_{\text{dep}}(t) = A \cdot t^B \cdot \exp(-t/C) \quad (7)$$

originally introduced for electromagnetic cascades [28]. The absorber depth t is measured in interaction lengths λ_i or radiation lengths X_0 for hadrons and electrons, respectively. B characterizes the growth of the cascade before the maximum and C the exponential decrease at large depths.

The number of low-energy ($1 - 10 \text{ GeV}$) muons increases as the shower develops then reaches a plateau because muons rarely interact. The attenuation of the muon component due to muon decay and energy loss is relatively slow. In contrast, the number of electrons and positrons declines rapidly after maximum because radiation and pair production subdivides the energy down to the critical energy ($E_c \sim 80 \text{ MeV}$ – see 5.3) after which electrons lose their remaining energy to ionization quickly. These basic features of longitudinal development of showers are illustrated in the right panel of Figure 16.1.

The left panel of Figure 16.1 shows the lateral distributions of the different components. Secondary hadrons are produced at a typical, almost energy-independent transverse momentum of $p_{\perp} \sim 350 - 400 \text{ MeV}$, leading to a large angle of low-energy hadrons relative to the shower axis. In contrast, most of the EM particles are in the cascades initiated by high-energy π^0 nearly parallel to the hadronic core. Their lateral spread comes mainly from multiple Coulomb scattering.¹ Thus the lateral distribution of muons is wider than that of EM particles because they are mainly produced in the decay of low-energy pions [505, 506]. For the same reason, hadronic interactions at low energy ($E \lesssim 200 \text{ GeV}$) largely determine the total muon yield [507, 508]. In round numbers the muons make up of order $\sim 10\%$ of the charged particles. In the EM component, the γ -rays outnumber the e^{\pm} by a factor of ~ 10 .

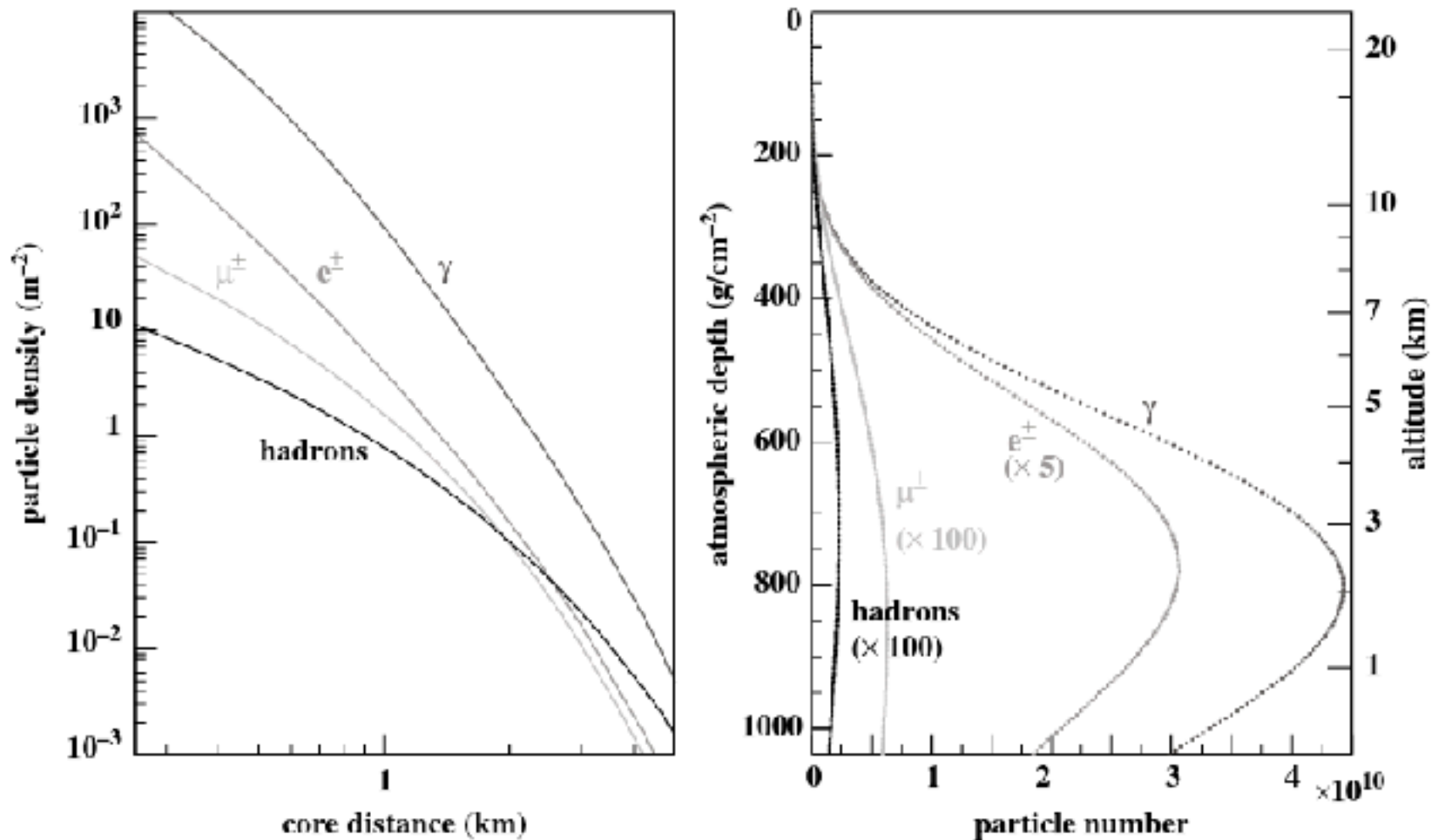
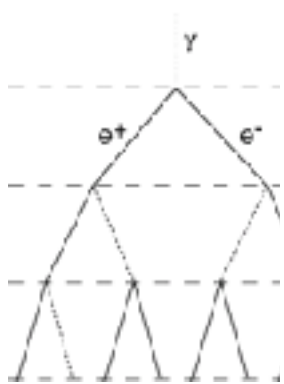


Figure 16.1 Average lateral and longitudinal shower profiles for vertical, proton-induced showers at 10^{19} eV. The lateral distribution of the particles at ground is calculated for 870 g/cm^2 , the depth of the Auger Observatory. The energy thresholds of the simulation were 0.25 MeV for γ , e^\pm and 0.1 GeV for muons and hadrons (from [33]).

A Matthews Heitler Model – Electromagnetic Cascades



pair production $\gamma \rightarrow e^+e^-$

bremsstrahlung $e \rightarrow e+\gamma$

splitting length $d=X_0 \ln 2$

radiation length $X_0=36.7 \text{ g/cm}^2$



Available online at www.sciencedirect.com

SCIENCE @ DIRECT®

Astroparticle Physics 22 (2005) 387–397

Astroparticle
Physics

www.elsevier.com/locate/astropart

A Heitler model of extensive air showers

J. Matthews *

Department of Physics and Astronomy, Louisiana State University, Baton Rouge, LA 70803, USA
Department of Physics, Southern University, Baton Rouge, LA 70813, USA

Received 8 August 2004; received in revised form 3 September 2004; accepted 13 September 2004
Available online 26 October 2004

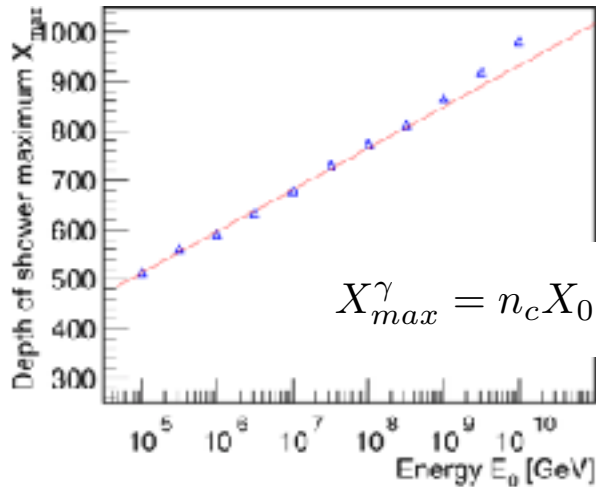
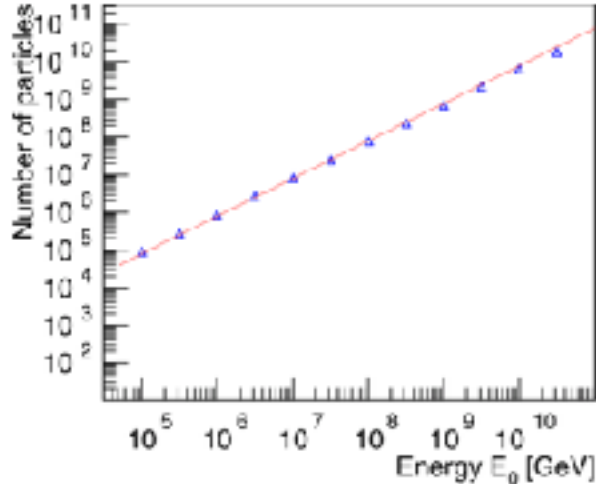
after n splitting lengths: $x = nX_0 \ln 2$ and $N = 2^n = \exp\left(\frac{x}{X_0}\right)$

energy per particle $E = E_0/N$ critical energy $E_c^e = 85 \text{ MeV}$

number of particles at shower maximum

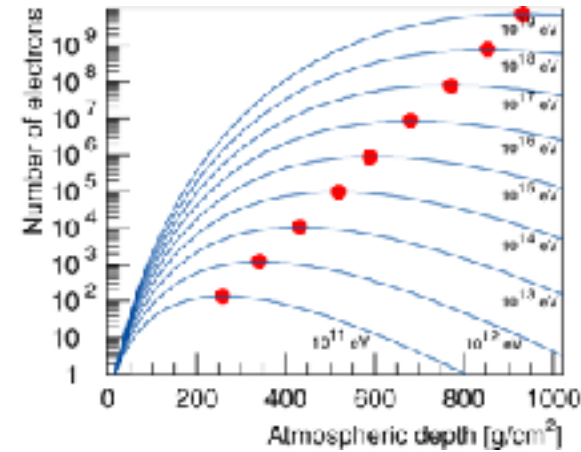
$$N_{max} = 2^{n_c} = \frac{E_0}{E_c^e} \quad n_c = \frac{\ln\left(\frac{E_0}{E_c^e}\right)}{\ln 2}$$

A Matthews Heitler Model – Electromagnetic Cascades



number of electrons at shower maximum

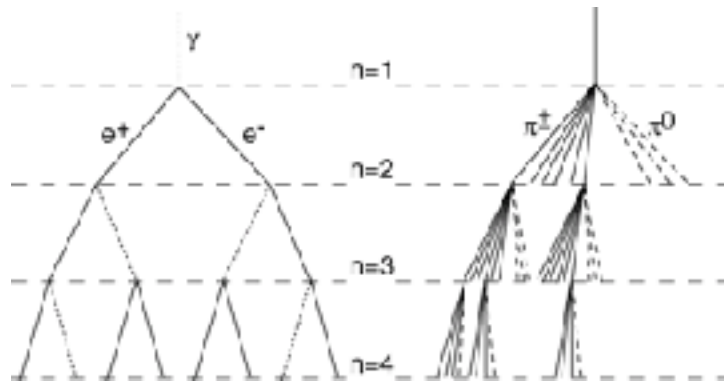
$$N_e^{max} = \frac{E_0}{gE_c^e} \approx 9.0 \cdot 10^5 \frac{E_0}{\text{PeV}} \quad g \approx 13$$



depth of shower maximum

$$X_{max}^\gamma = n_c X_0 \ln 2 = X_0 \ln \left(\frac{E_0}{E_c^e} \right) \approx 597 \frac{\text{g}}{\text{cm}^2} + 84 \frac{\text{g}}{\text{cm}^2} \lg \left(\frac{E_0}{\text{PeV}} \right)$$

A Matthews Heitler Model – Hadronic Cascades



hadronic interaction $\pi+A \rightarrow \pi^0 + \pi^+ + \pi^-$

interaction length $\lambda_{\pi\text{-air}} \sim 120 \text{ g/cm}^2$

π \rightarrow hadronic interaction
 \rightarrow decay

„critical energy“ $E_c^\pi \sim 20 \text{ GeV}$

in each interaction $3/2 N_{ch}$ particles: $N_{ch} \pi^{+-}$ and $1/2 N_{ch} \pi^0$ $N_{ch} \sim 10$

after n interactions $N_\pi = (N_{ch})^n$ $E_\pi = \frac{E_0}{\left(\frac{3}{2} N_{ch}\right)^n}$

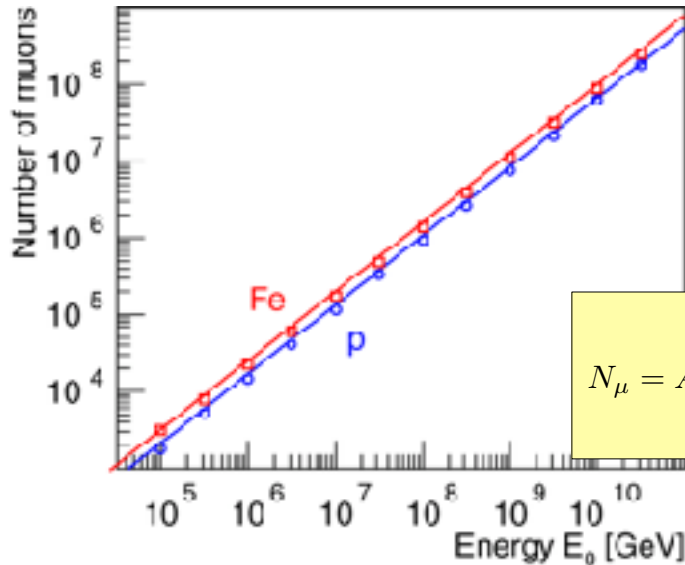
after n_c interactions $E_\pi = E_c^\pi$: $n_c = \frac{\ln E_0 / E_c^\pi}{\ln \frac{3}{2} N_{ch}} = 0.85 \lg \left(\frac{E_0}{E_c^\pi} \right)$

superposition model

particle $(E_0, A) \rightarrow A$ proton showers with energy E_0/A

A Matthews Heitler Model – N_μ and N_e

Number of muons at shower maximum

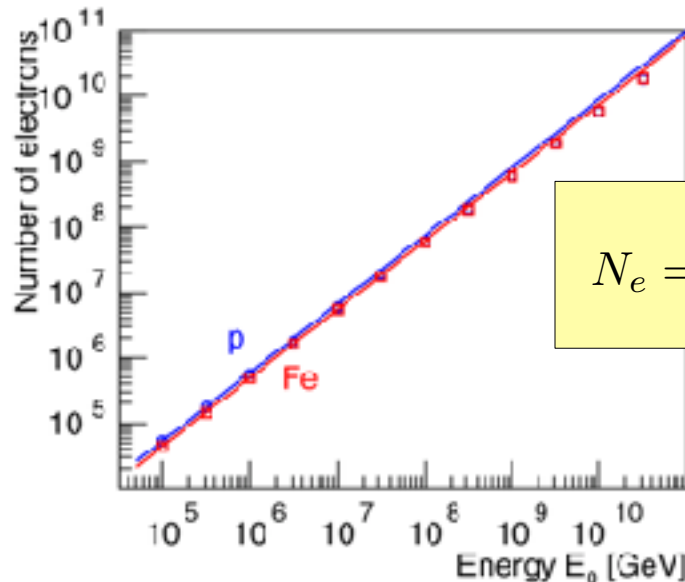


$$N_\mu = N_\pi = (N_{ch})^{n_c}$$

$$\ln N_\mu = n_c \ln N_{ch} = \beta \ln \left(\frac{E_0}{E_c^\pi} \right)$$

$$N_\mu = A \left(\frac{E_0}{AE_c^\pi} \right)^\beta = \left(\frac{E_0}{E_c^\pi} \right)^\beta A^{1-\beta} \approx 1.7 \cdot 10^4 \cdot A^{0.10} \left(\frac{E_0}{1 \text{ PeV}} \right)^{0.90}$$

Number of electrons at shower maximum



$$\frac{E_{em}}{E_0} = \frac{E_0 - N_\mu E_c^\pi}{E_0} = 1 - \left(\frac{E_0}{AE_c^\pi} \right)^{\beta-1}$$

$$N_e = \frac{E_{em}}{gE_c^e} \approx 6 \cdot 10^5 \cdot A^{-0.046} \left(\frac{E_0}{1 \text{ PeV}} \right)^{1.046}$$

A Matthews Heitler Model – N_μ vs. N_e

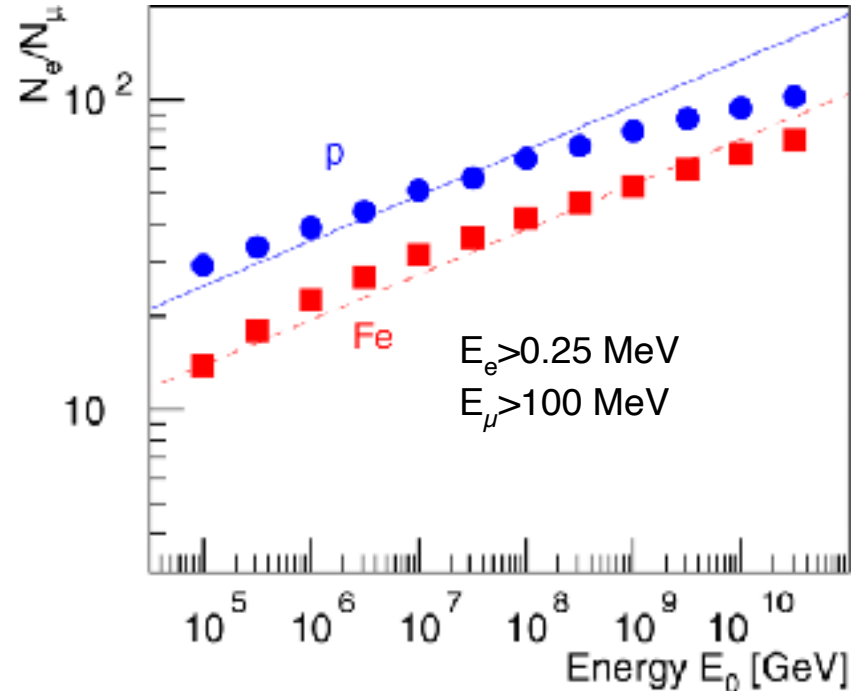
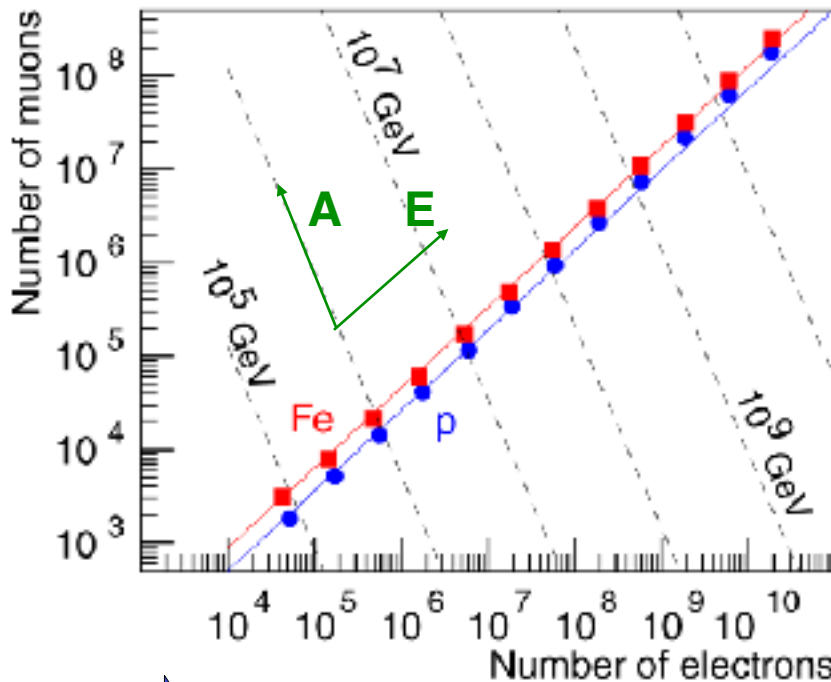
N_e - N_μ plane

$$N_\mu|_{A=\text{const}} \approx 0.18 A^{0.14} N_e^{0.86}$$

$$N_\mu|_{E_0=\text{const}} \approx 5.77 \cdot 10^{16} \left(\frac{E_0}{1 \text{ PeV}} \right) N_e^{-2.17}$$

N_e - N_μ ratio

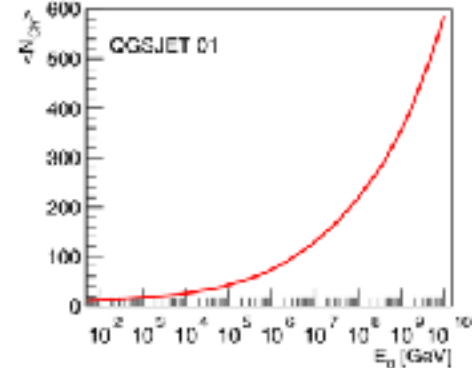
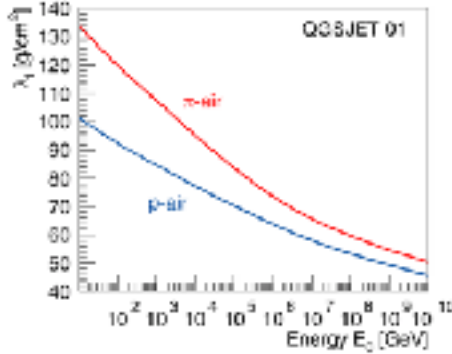
$$\frac{N_e}{N_\mu} \approx 35.1 \cdot \left(\frac{E_0}{A \cdot 1 \text{ PeV}} \right)^{0.15}$$



➡ estimator for mass A of primary particle

A Heitler Model – X_{max}

$$X_{max}^p = \lambda_i^{p-air} \ln 2 + X_0 \ln \left(\frac{\kappa E_0}{3N_{ch} E_c^e} \right)$$



proton air interaction length $\lambda_i^{p-air} = \xi + \zeta \lg \frac{E_0}{\text{PeV}} \quad \zeta = -4.88 \text{ g/cm}^2$

multiplicity of charged particles produced in π -N interactions

$$N_{ch} = N_0 \left(\frac{E_0}{\text{PeV}} \right)^\eta \quad \eta = 0.13$$

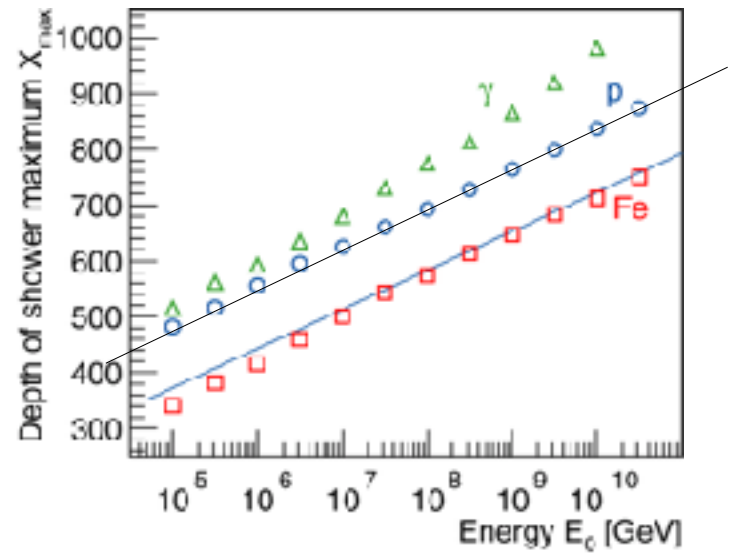
$$X_{max}^p = \xi \ln 2 - X_0 \left(\frac{3N_0 E_c^e}{\kappa \cdot \text{PeV}} \right) + \Lambda^p \lg \left(\frac{E_0}{\text{PeV}} \right)$$

elongation rate

e/m shower $\Lambda^\gamma = X_0 \ln 10 \approx 84.4 \text{ g/cm}^2$

proton shower

$$\Lambda^p = X_0 \ln 10 - \eta X_0 \ln 10 + \zeta \ln 2 \approx 70 \text{ g/cm}^2$$



X_{max} for heavy nuclei

$$X_{max}^A = X_{max}^p - X_0 \ln A$$

➡ estimator for mass A of primary particle

JRH, Mod. Phys. Lett. A 22 (2007) 1533

J. Matthews, Astrop. Phys. 22 (2005) 387

A Matthews Heitler Model – mass resolution in EAS measurements

depth of shower maximum


$$X_{\max}^A = X_{\max}^p - X_0 \ln A$$

radiation length $X_0=36.7 \text{ g/cm}^2$

typical uncertainty

$$\Delta X_{\max} \approx 20 \text{ g/cm}^2$$


expected mass resolution


$$\Delta \ln A \approx 0.8 - 1$$

electron-muon ratio

$$\lg(N_e/N_\mu) = C - 0.065 \ln A.$$

$$\Delta \frac{N_e}{N_\mu} \approx 16\% - 20\%$$



4 to 5 mass groups
p, He, CNO, (Si), Fe

16.3 Muons in air showers

Solution of the cascade equation 5.1 for EM particles was discussed in the previous chapter. Solving for single hadronic cascades is also possible by a combination of numerical integration and analytical expressions (see e.g. [511–514]). However the complexity of hadronic multiparticle production and the need to treat particle decays does not allow the derivation of compact analytic expressions for hadronic showers. With increasing computing power at hand it has become the standard to calculate hadronic showers numerically and to parametrize the results if needed. We will refer to the cascade equation framework in this chapter to illustrate some features of showers, while referring to results of full simulations as needed.

One-dimensional hybrid approach to extensive air shower simulation

2.2. Hadronic cascade equations

The backbone of a hadron-initiated extensive air shower is the hadronic cascade which develops via particle propagation, decay, and interaction with air nuclei of both the initial particle and of produced secondary hadrons. The corresponding integro-differential equations are given by [7] (see also [13])

$$\begin{aligned}
 \frac{\partial h_a(E, X)|_T}{\partial X} = & - \frac{h_a(E, X)|_T}{\lambda_a(E)} - h_a(E, X)|_T \frac{\left| \frac{dL}{dX} \right|_T}{\tau_a(E)c} \\
 & + \frac{\partial}{\partial E} (\beta_a^{\text{ion}}(E) h_a(E, X)|_T) \\
 & + \sum_d \int_E^{E_{\text{max}}} dE' h_d(E', X)|_T \left[\frac{W_{d \rightarrow a}(E', E)}{\lambda_d(E')} \right. \\
 & \left. + D_{d \rightarrow a}(E', E) \frac{\left| \frac{dL}{dX} \right|_T}{\tau_d(E')c} \right] + S_a^{\text{had}}(E, X)|_T, \quad (1)
 \end{aligned}$$

where $h_a(E, X)|_T$ are the differential energy spectra of hadrons of type a with energy E at depth position X along a given straight line trajectory T (in the following the T -symbol will be omitted), $\beta_a^{\text{ion}}(E) = -dE_a/dX$ is the ionization energy loss of particle a per depth unit. A muon is treated like a hadron, but without interaction term.

The first term in the r.h.s. of Eq. (1) represents the decrease of hadron number due to interactions with air nuclei

$$\frac{dh_a}{dX} = -\frac{h_a}{\lambda_a}, \quad (2)$$

with the corresponding mean free path $\lambda_a = m_{\text{air}}/\sigma_{\text{inel}}^{a\text{-air}}$, where m_{air} is the average mass of air molecules and $\sigma_{\text{inel}}^{a\text{-air}}$ is the hadron a -air nucleus inelastic cross section.

The second term describes particle decay, with the decay rate on a path dL being

$$dh_a = -h_a \frac{dL}{\tau_a c}, \quad (3)$$

where τ_a is the life time of hadron a in the lab. system, related to the proper life time $\tau_a^{(0)}$ by $\tau_a = \tau_a^{(0)}E/m_a$, with m_a being the hadron mass and c the velocity of light. From the definition of slant depth (28) follows

$$\left| \frac{dL}{dX} \right| = \frac{1}{\rho_{\text{air}}(X)}. \quad (4)$$

The third term in Eq. (1) takes into account particle ionization energy losses and the integral term in Eq. (1) represents the production of particles of type a in interactions and decays of higher energy parents of type d , with $W_{d \rightarrow a}(E', E)$, $D_{d \rightarrow a}(E', E)$ being the corresponding inclusive spectra of secondaries.

Finally, the so-called source term $S_a^{\text{had}}(E, X)$ defines the initial conditions and is determined during the MC simulation of above-threshold particle cascading. It consists of contributions of all sub-threshold hadrons produced at that stage

$$S_a^{\text{had}}(E, X) = S_a^{\text{MC} \rightarrow \text{had}}(E, X) = \sum_{i=1}^{N_{\text{source}}^{\text{had}}} \delta_{d_i}^a \delta(E - E_i) \delta(X - X_i) \quad (5)$$

with d_i , E_i , X_i being type, energy, and depth position of the source particles.

One-dimensional hybrid approach to extensive air shower simulation

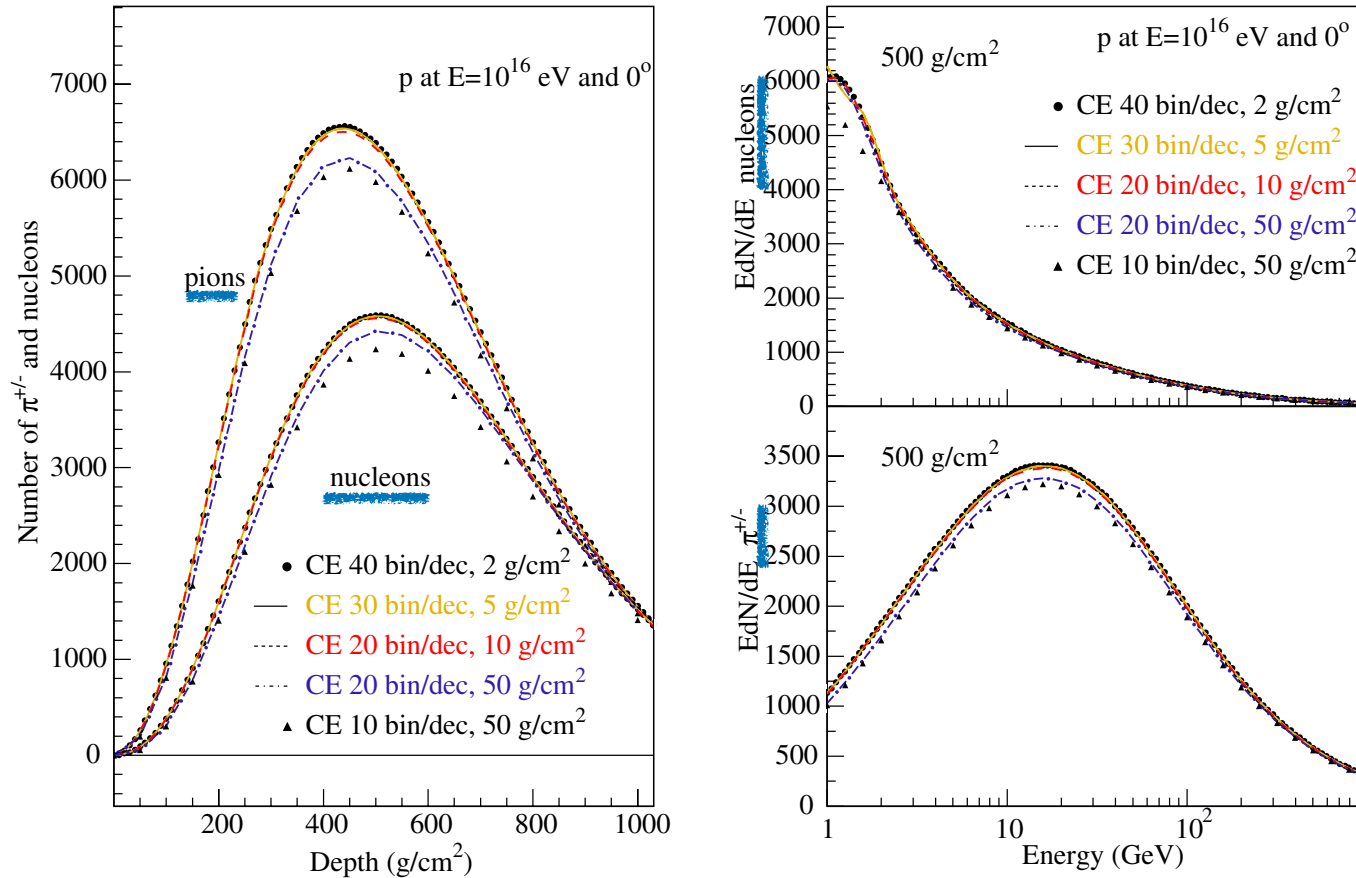


Fig. 1. Average hadronic shower size profiles (left panel) and energy spectra at $X = 500 \text{ g/cm}^2$ (right panel) of nucleons and charged pions for proton-initiated vertical ($\theta = 0^\circ$) showers of 10^{16} eV . Compared are the results of solving numerically the system of cascade equations (CE) with different discretization bin sizes in energy and depth.

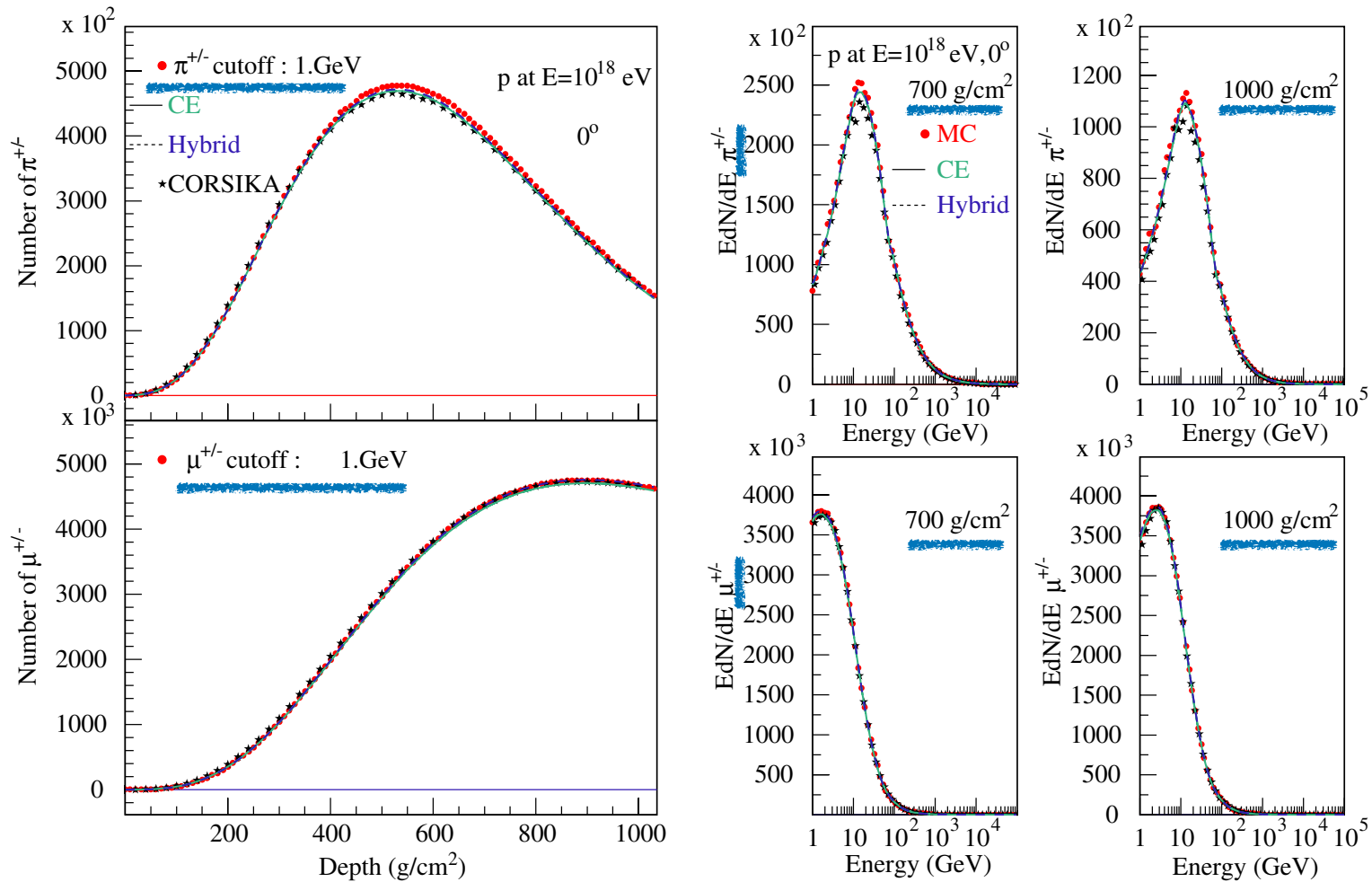


Fig. 2. Average longitudinal shower size profiles (left panel) and energy spectra (right panel) of charged pions and muons with energies above 1 GeV. The calculations were done for proton-initiated vertical showers of 10^{18} eV. Compared are the predictions obtained with CONEX applying the hybrid (dashed line), pure MC (points) and numerical calculation (full line) schemes. In addition CORSIKA predictions are shown as symbols (stars).

One-dimensional hybrid approach to extensive air shower simulation

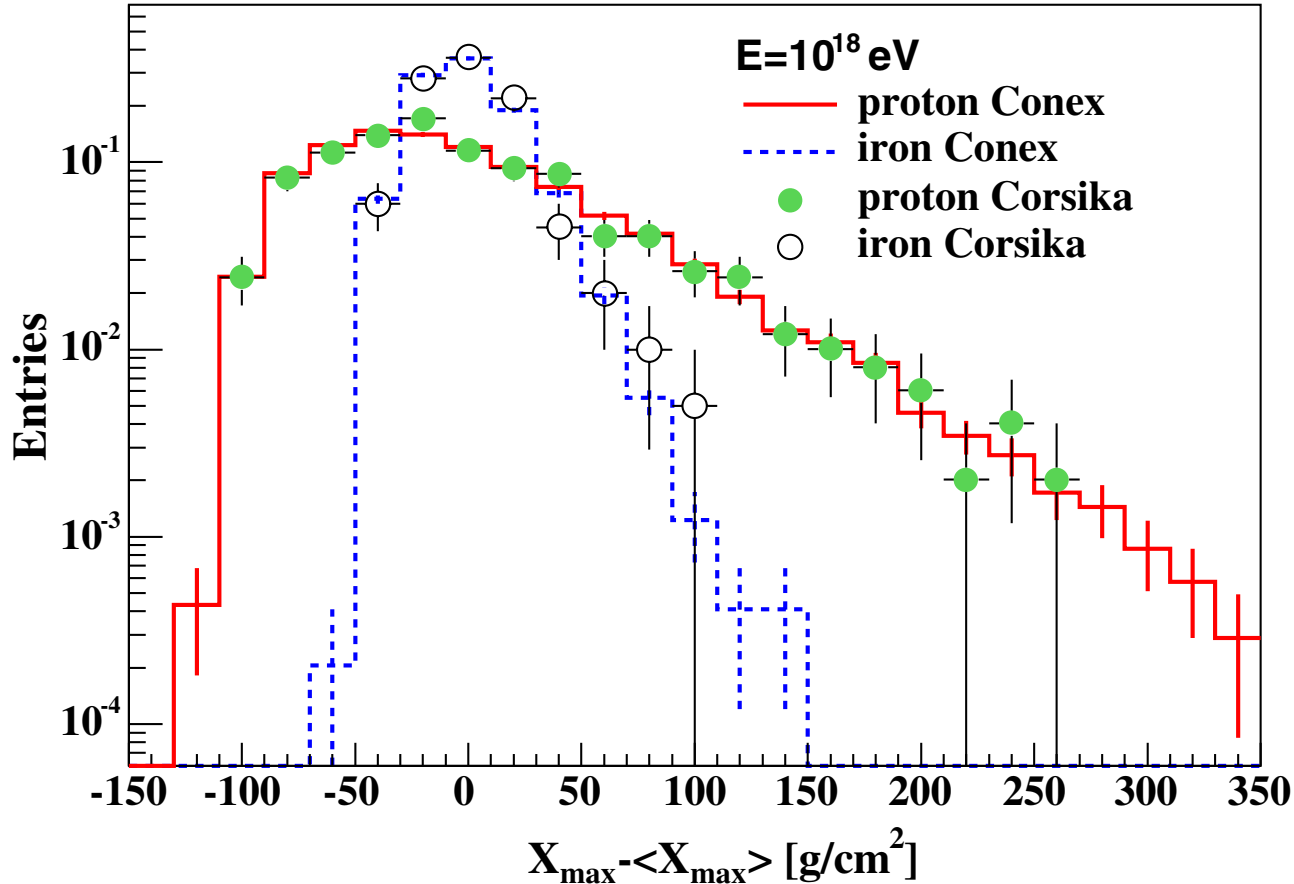


Fig. 7. Fluctuations of the shower maximum depth X_{\max} around corresponding mean shower maximum depths $\langle X_{\max} \rangle$ for a primary energy of 10^{18} eV for proton- and iron-initiated showers simulated with CONEX (lines) and CORSIKA (points).

Because the inclusive production functions (Eq. 5.4) to a good approximation depend only on the ratio of $E_{\text{secondary}}/E_{\text{beam}}$ in the forward fragmentation region, the yield of high-energy, stable secondary hadrons from a single primary proton can also be expected to scale. In other words, we expect the dimensionless combination to satisfy

$$E_i Y(E_i, E_0) = \mathcal{F}_i(\xi_i), \quad \text{with } \xi = \frac{E_i}{E_0}, \quad (16.6)$$

where $Y(E_i, E_0)$ is the differential yield of secondaries of energy E_i from a primary proton of energy E_0 . Here \mathcal{F}_i is integrated over slant depth as compared to Eq. 15.4.

The result of Eq. 16.6 can be used to get the form of the yield of high-energy muons in single air showers. The approximation will apply only for muon energy high enough so that decay of the parent mesons can be neglected in constructing Eq. 16.6. In practice this means TeV and higher ($E_\mu > \epsilon_\pi / \cos \theta$). From Eq. 5.61, we see that the probability of pion decay at a typical slant depth is proportional to $\epsilon_\pi / (E_\pi \cos \theta)$. (We illustrate here by considering only the contribution due to decay of charged pions. The kaon contribution has the same form.)

The function $F_{ji}(E_i, E_j)$ in Eq. 5.1 is the dimensionless particle yield that follows from the inclusive cross section (integrated over transverse momentum) for a particle of energy E_j to collide with an air nucleus and produce an outgoing particle i with energy $E_i < E_j$. In general, we define

$$F_{ji}(E_i, E_j) \equiv E_i \frac{1}{\sigma_j^{\text{air}}} \frac{d\sigma_{j \text{ air} \rightarrow i}}{dE_i} = E_i \frac{dn_i(E_i, E_j)}{dE_i}, \quad (5.4)$$

where dn_i is the number of particles of type i produced on average in the energy bin dE_i around E_i per collision of an incident particle of type j . All quantities in Eq. 5.4 are defined in the lab system. The relation to center-of-mass quantities can be derived from the definitions in Table 4.1. From Eq. 4.15 it follows that for energetic secondaries, i.e. those with $E_c \gg m_{T,c}$

$$E_c/E_a = x_L \approx x^*. \quad (5.5)$$

(We always define CMS as a projectile on a target *nucleon* even when that nucleon is bound in a nucleus, because nuclear binding energies will usually be much lower than energies of interest in cosmic ray problems we consider.)

muon spectrum from a primary proton of energy E_0 is obtained from convolution of the differential pion yield with the kinematic factor for $\pi^\pm \rightarrow \mu \nu_\mu$:

$$\frac{dN_\mu}{dE_\mu} = \int_{E_\mu}^{E_\mu/r_\pi} \frac{1}{E_\pi (1 - r_\pi)} \frac{\epsilon_\pi}{E_\pi \cos \theta} Y(E_\pi, E_0) dE_\pi, \quad (16.7)$$

where the kinematic limits are as in Eq. 6.18. Rewriting the equation in terms of the scaling variables $\xi_\pi = E_\pi/E_0$ and $\xi_\mu = E_\mu/E_0$, we get

$$\frac{dN_\mu}{d\xi_\mu} = \frac{\epsilon_\pi}{E_\mu \cos \theta} \xi_\mu F(\xi_\mu), \quad (16.8)$$

where

$$F(\xi_\mu) = \int_{\xi_\mu}^{\xi_\mu/r_\pi} \frac{\mathcal{F}(\xi_\pi)}{1 - r_\pi} \frac{d\xi_\pi}{\xi_\pi^3}.$$

Typically, we want the number of muons above an energy sufficient to reach a deep underground detector. The integral of Eq. 16.8 leads to

$$N_\mu(> E_\mu) = \frac{\epsilon_\pi}{E_\mu \cos \theta} \int_{\xi_\mu}^1 z F(z) dz = \frac{\epsilon_\pi}{E_\mu \cos \theta} G(\xi_\mu). \quad (16.9)$$

The same argument that leads to the scaling form for the yield of high-energy hadrons in a shower leads to a scaling approximation for the number of hadronic interactions in the shower. Such an approximation is

$$\frac{dn_{\text{int}}}{dz} \sim \delta(1-z) + \frac{1}{z} + 0.77 \frac{(1-z)^3}{z^{1.78}}, \quad (16.10)$$

where $z = E/E_0$ is the energy of the interaction scaled to the primary energy. The first two terms represent interactions of nucleons, the δ -function for the initial interaction and the $1/z$ term for subsequent interactions of nucleons assuming a flat distribution in fractional momentum for the reaction $N + \text{air} \rightarrow N + X$. The last term is due to interactions of mesons.

A check on energy conservation is useful to verify that formula 16.10, though rudimentary, is at least reasonable. Let $K_{\pi}^{(\gamma)}$ and $K_N^{(\gamma)}$ represent the fraction of the interaction energy that goes into the electromagnetic component in collisions respectively of π^\pm and nucleons. Then the total energy dumped into the electromagnetic component in all interactions is

$$\frac{E_{\text{tot}}}{E_0} = \sum_i K_i \int_0^1 z \frac{dn_i}{dz} dz = 2 K_N^{(\gamma)} + 2.41 K_{\pi}^{(\gamma)}, \quad (16.11)$$

where the sum is over two kinds of interactions, $i = N$ and $i = \pi^\pm$. Roughly, we expect half the energy of nucleon interactions to go into pions, of which approximately 1/3 is in neutral pions, so $K_N^{(\gamma)} \approx 1/6$. For pion-induced interactions the corresponding number should be somewhat less than 1/3. (If all outgoing particles were pions that shared equally in the energy, the number would be exactly 1/3; however, there is a tendency for the fastest produced pion to carry the charge of the pion that initiates the collision.) Energy conservation is satisfied by Eq. 16.11 if $K_N^{(\gamma)} \approx 1/6$ and $K_{\pi}^{(\gamma)} \approx 0.28$.

Assuming that most of the hadronic interactions are charged pions, the last term in Eq. 16.10 is equivalent to $\mathcal{F}(\xi_\pi) = 0.77(1 - \xi_\pi)^3(\xi_\pi)^{-0.78}$. Substitution of this form into Eqs. 16.8 and 16.9 leads to the result

$$G(\xi_\mu) \propto \left(\frac{E_0}{E_\mu} \right)^{0.78} \quad (16.12)$$

for $\epsilon_\pi \ll E_\mu \ll E_0$. A standard version of Eq. 16.9 that includes a threshold factor is

$$\langle N_\mu(> E_\mu) \rangle \approx A \times \frac{0.0145 \text{ TeV}}{E_\mu \cos \theta} \left(\frac{E_0}{A E_\mu} \right)^{0.757} \left(1 - \frac{A E_\mu}{E_0} \right)^{5.25}. \quad (16.13)$$

Here A is the mass of the parent nucleus, and the superposition approximation has been used, as explained in the next section.

The same starting point (Eq. 16.10) can also be used to obtain an approximation for the bulk of low-energy muons in air showers at the surface. For a simple estimate, assume that all charged pions with $E_\pi < \epsilon_\pi$ decay and all higher-energy charged pions interact. The spectrum of low-energy charged pions produced in the shower is then

$$\frac{dN_\pi}{dE_\pi} \sim \sum_i \int_{\epsilon_\pi}^{E_0} \frac{F_{i\pi^\pm}(x_\pi)}{E_\pi} \frac{dn_i}{dz} \frac{dE}{E_0}, \quad (16.14)$$

where $x_\pi = E_\pi/E$ and $F_{i\pi}$ is the inclusive cross section for $i \rightarrow \pi$ as defined in Eq. 5.4. Changing variables gives

$$\frac{dN_\pi}{dE_\pi} \sim \frac{1}{E_\pi} \sum_i \int_{\epsilon_\pi/E_0}^1 F_{i\pi^\pm}\left(\frac{E_\pi}{zE_0}\right) \frac{dn_i}{dz} dz. \quad (16.15)$$

For $E_\pi < \epsilon_\pi$ the integral can be approximated by evaluating the inclusive cross section at a small value of its argument where it is nearly constant. Furthermore, for $E_0 \gg \epsilon_\pi \approx 115 \text{ GeV}$, the integral is dominated by its most divergent term, so

$$\frac{dN_\pi}{dE_\pi} \sim \frac{1}{E_\pi} F_{\pi\pi}(0) \left(\frac{E_0}{\epsilon_\pi}\right)^{0.78}, \quad (16.16)$$

For $E_\pi < \epsilon_\pi$ the integral can be approximated by evaluating the inclusive cross section at a small value of its argument where it is nearly constant. Furthermore, for $E_0 \gg \epsilon_\pi \approx 115 \text{ GeV}$, the integral is dominated by its most divergent term, so

$$\frac{dN_\pi}{dE_\pi} \sim \frac{1}{E_\pi} F_{\pi\pi}(0) \left(\frac{E_0}{\epsilon_\pi} \right)^{0.78}, \quad (16.16)$$

where we have kept only the dominant meson interactions. The estimate for the total number of muons with $E_\mu > 1 \text{ GeV}$ in a nucleon-initiated shower, assuming one muon per pion, is obtained by integrating Eq. 16.16 up to $E_\pi \sim \epsilon_\pi$:

$$N_\mu(> 1 \text{ GeV}) \sim F_{\pi\pi}(0) \ln \epsilon_\pi (\text{GeV}) \left(\frac{E_0}{\epsilon_\pi} \right)^{0.78} \sim 10 \left(\frac{E_0}{\epsilon_\pi} \right)^{0.78}. \quad (16.17)$$

The numerical estimate comes from estimating

$$F_{\pi\pm\pi} = E_\pi \frac{dn_\pi}{dE_\pi} = \frac{dn_\pi}{d \ln E_\pi} \sim \frac{dn_\pi}{dy} \sim \frac{dn_\pi}{d\eta} \sim 2.$$

For comparison, the Akeno experiment [519] finds

$$N_\mu(> 1 \text{ GeV}) \approx 11 (E_0/\epsilon_\pi)^{0.83}. \quad (16.18)$$

Test of interaction models up to 40 PeV by studying hadronic cores of EAS

(The KASCADE Collaboration)

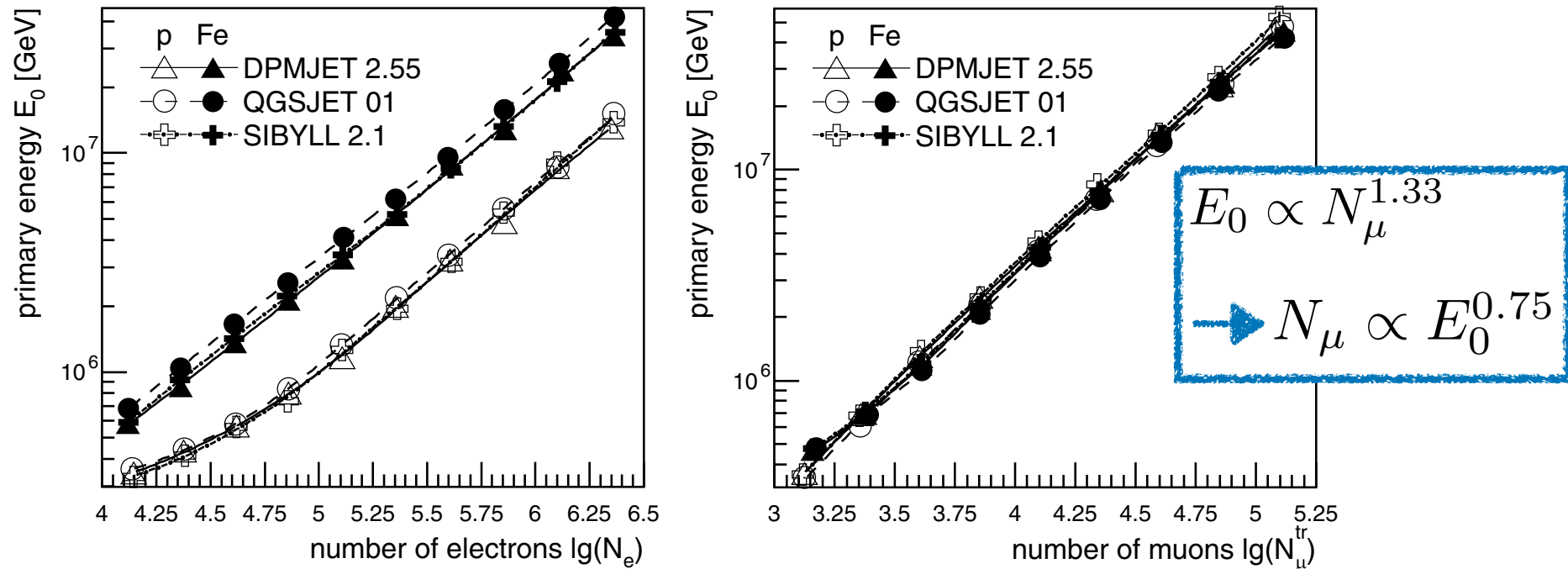
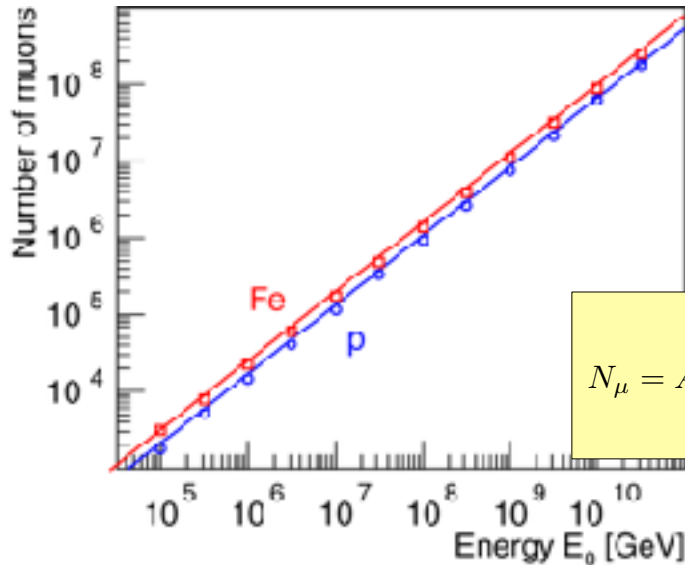


Figure 1. The mean primary energy for the interval of observed electron number N_e (left) and truncated muon numbers N_μ^{tr} (right). Results of simulations for protons and iron nuclei using the indicated high-energy interaction models are shown. The low-energy interactions have been treated by GHEISHA 2002. The lines are five parameter fits to guide the eyes.

A Matthews Heitler Model – N_μ and N_e

Number of muons at shower maximum

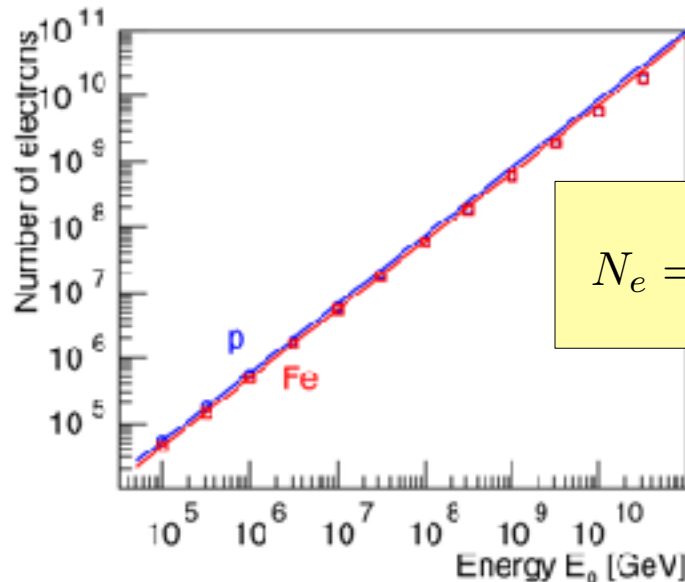


$$N_\mu = N_\pi = (N_{ch})^{n_c}$$

$$\ln N_\mu = n_c \ln N_{ch} = \beta \ln \left(\frac{E_0}{E_c^\pi} \right)$$

$$N_\mu = A \left(\frac{E_0}{AE_c^\pi} \right)^\beta = \left(\frac{E_0}{E_c^\pi} \right)^\beta A^{1-\beta} \approx 1.7 \cdot 10^4 \cdot A^{0.10} \left(\frac{E_0}{1 \text{ PeV}} \right)^{0.90}$$

Number of electrons at shower maximum



$$\frac{E_{em}}{E_0} = \frac{E_0 - N_\mu E_c^\pi}{E_0} = 1 - \left(\frac{E_0}{AE_c^\pi} \right)^{\beta-1}$$

$$N_e = \frac{E_{em}}{gE_c^e} \approx 6 \cdot 10^5 \cdot A^{-0.046} \left(\frac{E_0}{1 \text{ PeV}} \right)^{1.046}$$

16.4 Nuclei and the superposition model

With the binding energy of ~ 5 MeV per nucleon being much smaller than the typical interaction energies, one can consider a nucleus of mass A approximately as A independent nucleons. In this superposition model, a nucleus with mass A and energy E_0 is considered as A independent nucleons with energy $E_h = E_0/A$. This leads to the predictions

$$\begin{aligned} N_{\text{em,max}}^A(E_0) &= A \cdot N_{\text{em,max}}^h(E_h/E_c) \approx N_{\text{em,max}}(E_0) \\ X_{\text{max}}^A(E_0) &= X_{\text{max}}(E_0/A) \\ N_{\mu}^A(E_0) &= A \cdot \left(\frac{E_0/A}{E_{\text{dec}}} \right)^{\alpha} = A^1 \propto \left(\frac{E_0}{E_{\text{dec}}} \right)^{\alpha}. \end{aligned} \quad (16.19)$$

From the first line of this equation, we see that if the fraction of energy transferred to the EM shower component were independent of energy there would be no mass dependence of the number of charged particles at shower maximum. In contrast, from the second and third lines, we expect that the depth of maximum and the number of muons both depend on the mass of the primary particle. (Compare Eqs. 16.3 and 16.5.) The heavier the shower-initiating particle the more muons are expected for a given primary energy and the shallower the depth of maximum. Iron showers contain about 40% more muons than proton showers of the same energy and reach their maximum 80 – 100 g/cm² higher in the atmosphere.

One of the important aspects of the superposition model is the fact that, averaged over many showers, the distribution of nucleon interaction points in the atmosphere coincides with that of more realistic calculations accounting for nucleus interactions and breakup into remnant nuclei [520]. Therefore it is not surprising that the superposition model gives a good description of many features of air showers if inclusive observables are concerned such as the mean depth of shower maximum and the number of muons. However, it is not applicable to observables related to correlations or higher order moments [521, 522].

In the superposition approximation according to Eq. 16.19, the relation between primary energy and number of particles at the position of maximum shower development (X_{\max}) is independent of the mass of the primary nucleus, but the position of X_{\max} depends on primary mass as

$$X_{\max} \propto \lambda \ln[E_0/(A E_c)]. \quad (16.20)$$

This equation is a version of the elongation rate theorem to be discussed in the next section. It has the implication that showers generated by heavy primaries develop more rapidly on average (i.e. higher in the atmosphere) than proton showers of the same total energy. On the other hand, the effect is only logarithmic, so it is clear, given the nature of air shower experiments, that the best one can hope for is to be able to distinguish among groups of nuclei with quite different masses. In practice, even this has proved difficult. Another important distinguishing feature of showers generated by heavy nuclei is that fluctuations in their longitudinal development are smaller than those of light nuclei. This is simply because each nucleus is a beam of many incident nucleons.

In reality what happens when a heavy nucleus enters the atmosphere is that it interacts very quickly (recall, for example, that $\lambda \sim 2.3 \text{ g/cm}^2$ for an iron nucleus). In this first collision, however, only a few of the nucleons in the nucleus interact inelastically with an air nucleus to create secondary pions. Several other nucleons and light nuclear fragments may also be released, and there will generally be one heavy fragment. By studying fragmentation histories of nuclei in photographic emulsion and the multiplicities of secondary particles produced in the various fragmentation events, it is possible to build up a more realistic picture of how nuclei break up in the atmosphere and when their constituent nucleons first interact. The procedure is complicated and very approximate, but it serves to give an indication of the reliability of the superposition model. One complication with the analysis is that a subset of the interactions that correspond with interactions on the light nuclei in the emulsion must be selected since the atmosphere consists almost entirely of light nuclei. Another is that there may be a selection bias for events with higher multiplicity. As a consequence, the estimate of the number of nucleons that interact to produce pions may be somewhat overestimated. Figure 16.3 shows the distribution of points of first interaction for the superposition model as compared to that inferred from the data. The distributions become steeper at higher energy because of the increase with energy of the nucleon cross section.

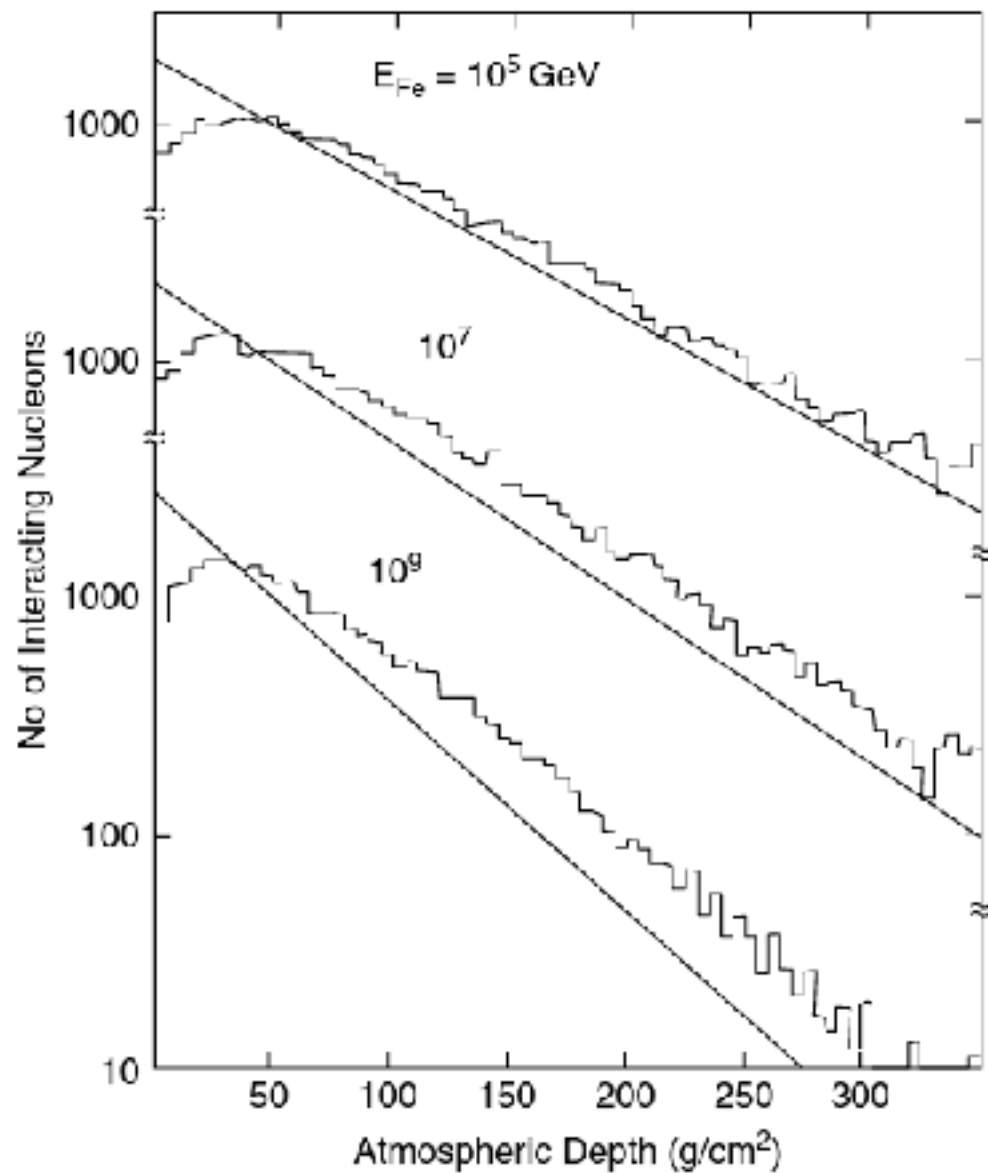


Figure 16.3 Distribution of points of first interaction for nucleons in iron nuclei. Histograms: inferred from data in photographic emulsion. Lines: superposition model. (From Ref. [523])

The general idea of reducing a nucleus-nucleus collision to a series of nucleon-nucleon collisions is called the “wounded nucleon” picture. A simplified version can be constructed directly from the impact parameter representation for the total inelastic cross section from Eq. 4.85. For a proton–nucleus interaction, the total inelastic cross section can be developed as a sum of partial cross sections for exactly N wounded nucleons, see Eqs. 4.83 and 4.85,

where

$$\sigma_N = \int d^2b \frac{[\sigma T(b)]^N}{N!} \exp[-\sigma T(b)],$$

and σ is the nucleon–nucleon cross section. The mean number of wounded nucleons in the target (i.e. the number of nucleon–nucleon collisions) is

$$\langle N \rangle_{pA} = \frac{A \sigma_{pp}}{\sigma_{pA}}.$$

For a nuclear projectile of mass A incident on a target nucleus of mass B the generalization is [524]

$$\langle N \rangle_{AB} = \frac{A \sigma_{pB}}{\sigma_{AB}} + \frac{B \sigma_{pA}}{\sigma_{AB}}.$$

The first term is the number of wounded nucleons in the projectile and the second the number of wounded nucleons in the target. This simple geometrical result predicts that a somewhat larger fraction of the freed nucleons interact to produce pions than the analysis of emulsion data described above.

Considering hadron–nucleus interactions, an approximate and much simpler version of the full Glauber theory is represented by the formula

$$\sigma_{\text{ine}}^{hA} = \int d^2b \{1 - \exp[-\sigma_{\text{tot}}^{hp} T(b)]\}, \quad (4.83)$$

which is the extension of (4.72) to nuclear targets. Here σ_{ine}^{hA} is the inelastic cross section for hadron–nucleus scattering and σ_{tot}^{hp} is the corresponding total hadron–nucleon cross section. The function $T(b)$ is the number density of target nucleons of the nucleus at impact parameter b , folded with the impact parameter profile of the amplitude for hadron–nucleon scattering (see Eq. 4.67)

$$T(b) = \int \rho_N(\vec{r}) A_{hp}(\vec{b} - \vec{b}_N) dz d^2b_N, \quad (4.84)$$

where ρ_N is the number density of nucleons at distance $r = \sqrt{b_N^2 + z^2}$ from the center of the nucleus. The production cross section $\sigma_{\text{prod}}^{hA}$ is given by an expression very similar to (4.83) [175]

$$\sigma_{\text{prod}}^{hA} = \int d^2b \{1 - \exp[-\sigma_{\text{ine}}^{hp} T(b)]\}. \quad (4.85)$$

Two limits follow directly from (4.85). If $\sigma_{\text{ine}}^{hp} T(b)$ is very small then there is no “shadowing”, and

$$\sigma_{\text{prod}}^{hA} \approx \int \sigma_{\text{ine}}^{hp} T(b) d^2b = A \sigma_{\text{ine}}^{hp}. \quad (4.86)$$

In the opposite limit of complete screening ($\sigma_{\text{ine}}^{hp} T(b)$ very large) the integrand of (4.85) is approximately unity out to an effective nuclear radius R_A , so

$$\sigma_{\text{prod}} \approx \pi R_A^2 \propto A^{2/3}. \quad (4.87)$$

In the range of beam momentum 20 – 50 GeV/c, the A -dependence of σ_{ine}^{pA} for $A > 1$ can be approximated by (see [176])